Kinetics of phase separation in the driven lattice gas: Self-similar pattern growth under anisotropic nonequilibrium conditions

P. I. Hurtado,[1] J. Marro,[1] P. L. Garrido,[1] and E. V. Albano[2]
[1]*Instituto Carlos I de Física Teórica y Computacional, and Departamento de Electromagnetismo y Física de la Materia, Universidad de Granada, 18071 - Granada, Spain*
[2]*Instituto de Investigaciones Fisicoquímicas Teóricas y Aplicadas, UNLP, CONICET, La Plata, Argentina*
(Received 27 May 2002; revised manuscript received 9 October 2002; published 29 January 2003)

The driven lattice gas (DLG) evolving at low temperature helps understand the kinetics of pattern formation in unstable mixtures under anisotropic conditions. We here develop a simple theoretical description of kinetics in Monte Carlo simulations of the DLG. A Langevin continuum analog is also studied which is shown to exhibit the same behavior. We demonstrate that pattern growth is mainly a consequence of single-particle processes and that, after a short transient time, in which a surface evaporation/condensation mechanism is important, hole diffusion in the bulk becomes dominant. Consequently, there is a unique relevant length that behaves $\ell(t)\sim t^{1/3}$ for macroscopic systems except at some very early (perhaps unobservable) time. This implies a sort of self-similarity, namely, the spatial pattern looks alike, but for a (nontrivial) change of scale at different times. We also characterize the structure factor, in which we identify Guinier and Porod regions, and its scaling form with both time and size. The underlying anisotropy turns out to be essential in determining the macroscopically emergent peculiar behavior.

DOI: 10.1103/PhysRevB.67.014206 PACS number(s): 61.20.Ja, 05.20.Dd, 64.60.Qb

I. INTRODUCTION

Many alloys such as Al-Zn, which are homogeneous at high temperature, undergo phase separation after a sudden quench into the miscibility gap (for details, see the reviews in Refs. 1–5, for instance). One first observes nucleation in which small localized regions (*grains*) form. This is followed by ''spinodal decomposition.'' That is, some grains grow at the expense of smaller ones, and eventually coarsen, while their composition evolves with time. In addition to being theoretically challenging, the details are of great practical importance. For example, hardness and conductivities are determined by the spatial pattern finally resulting in the alloy, and this depends on how phase separation competes with the progress of solidification from the melt.

A complete kinetic description of these highly nonlinear processes is lacking.[5] Nevertheless, the essential physics for some special situations is now quite well understood. This is the case when nothing prevents the system from reaching the equilibrium state, namely, coexistence of two thermodynamic phases. The simplest example of this is the (standard) lattice gas evolving from a fully disordered state to segregation into *liquid* (particle-rich phase) and *gas* (particle-poor phase). (Alternatively, using the language of the isomorphic lattice binary alloy,[6] the segregation is into, say Al-rich and Zn-rich phases.) As first demonstrated by means of computer simulations,[1,2,7] this segregation, as well as similar processes in actual mixtures, exhibit time *self-similarity*. This property is better defined at sufficiently low temperature, when the thermal correlation length is small. The system then exhibits a *single* relevant length, the size $\ell(t)$ of typical grains growing algebraically with time. Consequently, any of the system properties (including the spatial pattern) look alike, except for a change of scale, at different *times*.

This interesting property is revealed, for example, by the sphericalized structure factor $S(k,t)$ as observed in scattering experiments. After a relatively short transient time, one observes that $S(k,t)\sim J(t)\cdot F[k\ell(t)]$. Taking this as a hypothesis, one may interpret J and l as phenomenological parameters to scale along the S and k axes, respectively. The hypothesis is then widely confirmed, and it follows that $J(t)\sim\ell(t)^d$ where d is the system dimension. It also follows that $F(\varkappa)=\Phi(\varkappa)\cdot\Psi(\sigma\varkappa)$ where Φ and Ψ are universal functions. In fact, Φ describes the diffraction by a single grain, Ψ is a grain interference function, and σ characterizes the point in the (density-temperature) phase diagram where the sample is quenched. It then ensues that $\Psi\approx 1$ except at small values of k, so that, for large $\varkappa$, $F(\varkappa)$ becomes almost independent of density and temperature, and even the substance investigated.[5,7,8]

The grain distribution may also be directly monitored. A detailed study of grains in both microscopy experiments and computer simulations confirms time scale invariance. More specifically, one observes that the relevant length grows according to a simple power law, $\ell(t)\sim t^a$, and one typically measures $a=\frac{1}{3}$ at late times. This is understood as a consequence of diffusion of monomers that, in order to minimize surface tension, evaporate from small grains of high curvature and condensate onto larger ones (Ostwald ripening). In fact, Lifshitz, Slyozov, and Wagner independently predicted $\ell\sim t^{1/3}$,[9] which is often observed, even outside the domain of validity of the involved approximations.[10] In some circumstances, one should expect other, nondominant mechanisms inducing corrections to the Lifshitz-Slyozov-Wagner one.[1,3,5] For instance, effective diffusion of grains (Smoluchowski coagulation) leads to $a=\frac{1}{6}$, which may occur at early times;[11] interfacial conduction leads to $a=\frac{1}{4}$;[12,13] and, depending on density and viscosity, a fluid capable of hydrodynamic interactions may exhibit crossover with time to viscous ($a=1$) and then inertial ($a=\frac{2}{3}$) regimes.[4]

Whether one can extend the above interesting picture to more realistic situations is an open question. The assumption that the system asymptotically tends to the coexistence of two *thermodynamic* (equilibrium) phases is often unjustified in nature. This is the case, for example, for mixtures under a shear flow, whose study has attracted considerable attention, e.g., see Refs. 14–18. The problem is that sheared flows asymptotically evolve towards a *nonequilibrium* steady state and this is highly anisotropic. Studying the consequences of anisotropy in the behavior of complex systems is in fact an important challenge (see, for instance, Refs. 19–21). Another important example is that of binary granular mixtures under horizontal shaking. The periodic forcing causes in this case phase separation and highly anisotropic clustering.[46]

In this paper, we study in detail the kinetics of the driven lattice gas[20] (DLG) following a deep quench. Our motivation is twofold. On one hand, the DLG is recognized to be an excellent microscopic model for nonequilibrium anisotropic phenomena.[21] On the other, the DLG is not affected by hydrodynamic interactions, which makes physics simpler. Our goal is timely given that the asymptotic state of the DLG is now rather well understood, and previous studies of kinetics altogether reveal an intriguing situation.[21–28] Following this pioneering effort, we here present a theoretical description of the essential physics during anisotropic, nonequilibrium pattern growth. This is compared with extensive computer simulations. A brief and preliminary account of some of our results was presented elsewhere.[29]

II. MODEL AND SIMULATION DETAILS

The DLG consists of a d-dimensional, e.g., simple cubic lattice with configurations $\mathbf{n}=\{n_i;i=1,\ldots,N\}$. The variable at each lattice site has two possible states, $n_i=1$ (particle) or 0 (hole). As for the standard lattice gas, dynamics is a stochastic process at temperature T consisting of nearest-neighbor (NN) particle/hole exchanges. This conserves the particle density, $\rho=N^{-1}\Sigma_i n_i$, and depends on $\mathbf{n}$.

A distinguishing feature of the DLG is that exchanges are favored in one of the principal lattice directions, say, $\vec{x}$. Therefore, assuming periodic (toroidal) boundary conditions, a net current of particles is expected to set in along $\vec{x}$. This is accomplished in practice by defining a biased transition rate. We shall refer here to the *energy* function $H=-4J\Sigma_{NN}n_i n_j$, which describes attractive interactions between particles at NN sites, and to the transition rate (per unit time):[21]

$$\omega(\mathbf{n}\rightarrow\mathbf{n}^*)=\min\{1,e^{-(\Delta H+E\delta)/T}\}. \tag{1}$$

$\mathbf{n}^*$ stands for configuration $\mathbf{n}$ after jumping of a particle to a NN hole, $\Delta H=H(\mathbf{n}^*)-H(\mathbf{n})$ is the energy change brought about by the jump, and units are such that both the coupling strength J and the Boltzmann constant are set to unity. One further defines $\delta=(\mp 1,0)$ for NN jumps along $\pm\vec{x}$ or along any of the transverse directions, say, $\vec{y}$, respectively. Consistent with this, $\vec{E}=E\vec{x}$ may be interpreted as field driving particles, e.g., an electric field if one assumes that particles are charged. (One may adopt other interpretations, e.g., the binary alloy one.[6] Dynamics then consists of interchanges between particles of different species, one of them favored along $\vec{x}$.)

The DLG was described as modeling surface growth, fast ionic conduction, and traffic flow, among a number of actual situations of practical interest.[21] A common feature in these situations is anisotropy, and that steady states are out of equilibrium. Both are essential features of the DLG induced by the rate (1). The only trivial case is for $E=0$, which reduces (1) to the Metropolis algorithm. In this case, detailed balance holds, and one simply has the familiar lattice gas with a unique (equilibrium) steady state. For any, even small E, qualitatively new behavior emerges. In fact, detailed balance breaks down for $E>0$ and, consequently, the steady state depends on $\omega(\mathbf{n}\rightarrow\mathbf{n}^*)$. Increasing E, one eventually reaches saturation. That is, particles cannot jump backwards, i.e., $-\vec{x}$, which formally corresponds to an infinite field ($E=\infty$).

The way in which the microscopic anisotropy (1) conveys into macroscopic behavior is amazing.[21] Consider, for simplicity, $d=2$, $\rho=\frac{1}{2}$, and $E=\infty$. The system then exhibits a critical point at $T=T_C^{\infty}\simeq 1.4T_C(E=0)$, where $T_c(E=0)\approx 2.2691$, with different critical behavior.[27,28] Furthermore, the asymptotic, steady states below T_C^{∞} do not comprise equilibrium phases. Instead, one observes a particle current and fully anisotropic phases; both are nonequilibrium features. The intensity of the current increases with T, and suddenly changes slope at T_C^{∞} (in fact, this property may serve to accurately locate the critical point). The stable ordered configurations consist of one stripe, to be interpreted as a *liquid* (rich-particle) phase of density $\rho_L(T)$. The *gas* (poor-particle) phase of density $\rho_G(T)$ fills the remainder of the system. Except for some microscopic roughness, the interface is linear and rather flat, in general.[30]

The computer evolutions reported here always begin with a completely disordered state to simulate the system at infinite temperature. We then model a sudden quench and the subsequent time evolution. With this aim, one proceeds with a rate (1) that involves the temperature T at which the system is quenched. The run is followed until one stripe is obtained (eventually, in order to save computer time, the run was sometimes stopped before reaching the final stationary state). The code involves a list of $\eta(t)$ particle-hole NN pairs from where the next move is drawn. Time is then increased by $\Delta t=\eta(t)^{-1}$, so that its unit or Monte Carlo (MC) step involves a visit to all sites on the average.[32]

The lattice is rectangular, $L_{\parallel}\times L_{\perp}$, with sides ranging from 64 to 256 and, in a few cases, 512. Results concern on average over around a thousand independent runs. Due to the great computational effort which is consequently involved, this paper describes simulations concerning a single point of the two-dimensional DLG phase diagram. That is, most of our evolutions are for $\rho=\frac{1}{2}$ and $E=\infty$, and simulate a quench at $T=0.8T_C$ $(E=0)\simeq 0.6T_C^{\infty}$. This choice is motivated by the fact that clustering is then reasonably compact, which helps to obtain good statistics, while it proceeds fast enough, so that one can observe full relaxation to the steady state. In spite of this restriction, brief investigation of other

points, together with some of our observations below, led us to believe that the validity of our results extends to a large domain around the center of the miscibility gap; in fact, such generality of behavior has been reported for $E=0$.[2,5,7,11]

III. GROWTH OF ORDER

The DLG exhibits different time regimes during phase separation. Though they parallel the ones for $E=0$, the peculiarities induced by the anisotropic condition are essential.

Starting from complete disorder, there is a very short initial regime in which small grains form. The novelty is that typical grains are now fully anisotropic, stretched along $\vec{x}$. The grains then rapidly coarsen to form macroscopic strings, as illustrated in Fig. 1. Sheared fluids (an experimentally accessible situation that also involves both nonequilibrium physics and anisotropy) seem to exhibit similar initial regimes.[16,18] That is, during a short-time interval, they show larger growth rate along the flow than in the other directions, which is assumed to correspond to the initial formation of anisotropic regions. Afterwards, sheared fluids develop stringlike macroscopic domains similar to the ones in the DLG.

Figure 1 includes a comparison with the zero-field case, i.e., the standard, isotropic lattice gas (LG). This clearly illustrates the strong anisotropy of nucleation and early phase separation for the DLG. Close inspection of these and similar graphs also seems to indicate relatively small but significant differences in the degree of segregation between the two cases at a given time. That is, at small distances, there is a more homogeneous distribution of particles, both longitudinally and transversely, in the DLG than in the LG. The latter shows to be more segregated at the same time, which is already rather evident by direct inspection of graphs for $1<t\leqslant 100$ in Fig. 1. We believe this reveals the different role played by surface tension as the degree of anisotropy is varied: Typical DLG grains are rather linear except at their longitudinal ends, where curvature may be even stronger than for the spherical clusters in the LG at comparable times. This seems to be at the origin of a smoother transverse distribution of particles in the DLG at early times. On the other hand, the field also tends to smoothen things longitudinally.

In order to quantify the aforementioned observation, we evaluated the number of broken bonds in the direction of (perpendicular to) the field, $n_{\parallel}(t)$ $[n_{\perp}(t)]$, as a function of time during the early evolution stage. Then $A(t)\equiv[n_{\perp}(t)+n_{\parallel}(t)]/2N$ is the density of broken bonds. The higher the degree of segregation at time t, the smaller is $A(t)$. For instance, we observe in a large 256×256 lattice that $A(t=10)=0.295$ and $A(t=10)=0.38$ for the LG and DLG, respectively, confirming the above observation. On the other hand, let $B(t)\equiv[n_{\perp}(t)-n_{\parallel}(t)]/2N$. One would expect $B(t)\approx 0$ (up to fluctuations) only for the isotropic system. In fact, we measured $B(t)\approx 0$ for the LG, while $B(t)$ rapidly converges to a nonzero value $B(t)\approx 0.05$ for the DLG at early times (again for a large 256×256 lattice). We take this number, $B(t)=0.05$, as characterizing the anisotropic shape of DLG clusters at early times.

The difference of segregation between the DLG and the LG at early times merits further study. This will need to take into account the anisotropy of surface tension. In any case, this concerns a regime very near the initial, melt state that only bears minor practical importance, given that it extends extremely shortly on the macroscopic time scale. We are interested in the rest of this paper on the subsequent evolution, to be described on the assumption of a simple flat interface, which holds in Fig. 1 for $t>100$.

The DLG strings coarsen with time until well-defined, relatively narrow longitudinal (i.e., directed along $\vec{x}$) stripes are formed. (For periodic boundary conditions, the case of our simulations, each stripe forms a ring.) This results into a multistripe state, as illustrated in Figs. 1 and 2. The ordering time in the DLG, defined as the time the system needs to form the stripes, scales with the system size in the direction of the field, $L_{\parallel}$, since in this case ordered clusters (stripes) percolate along the field direction (see below).[26] This is not the case for the equilibrium LG, where the ordering time depends exclusively on system-intensive parameters such as temperature and density.

The multistripe states are not stable, however. They are only partially segregated and, in fact, a definite tendency towards a fully segregated state with a single stripe is generally observed in computer simulations. One may also develop simple arguments indicating that, in general, a multistripe state will monotonically evolve until forming a single stripe.[21,33] It is true that, in practice, the complete relaxation may take a very long time. More specifically, a macroscopic system may take to decay into the true stable state a long, macroscopic time interval, namely, a time that may show up as mathematically infinite in some time scales. In fact, the complete relaxation time is observed to increase with system size, as first demonstrated in Ref. 26. It should also be remarked that this property is not a nonequilibrium feature but occurs already in the equilibrium $(E=0)$ case; see, for instance, Refs. 2 and 4, and references therein. Slow relaxation is a consequence of the conservation of particle density ρ implied by the particle-hole exchange dynamics; this induces scale invariance, namely, slow (power-law) evolution of correlations so that, once enough order sets in, all but very small pattern modifications during a single MC step are precluded. Consequently, certain individual runs sometimes block for a long time in a state with several stripes; however, this does not correspond to the average behavior. As illustrated by Fig. 2, which shows a typical evolution, and demonstrated below by our averages corresponding to thousand evolutions, the number of stripes monotonically decreases with time (see also Sec. V), and the whole relaxation can easily be observed in computer simulations if one waits long enough.

We next attempt a theoretical description of the relaxation process. Our interest is on the *anisotropic spinodal decomposition* by which the earliest state with many well-defined stripes decays into a single stripe. We shall assume that relaxation is a consequence of monomer events causing effective diffusion of liquid stripes. (Note that assuming gas stripes here would be completely equivalent.) That is, due to single-particle processes, liquid stripes move transversely as a whole, and may collide and eventually coalesce with one of the neighboring stripes; see the late evolution depicted in

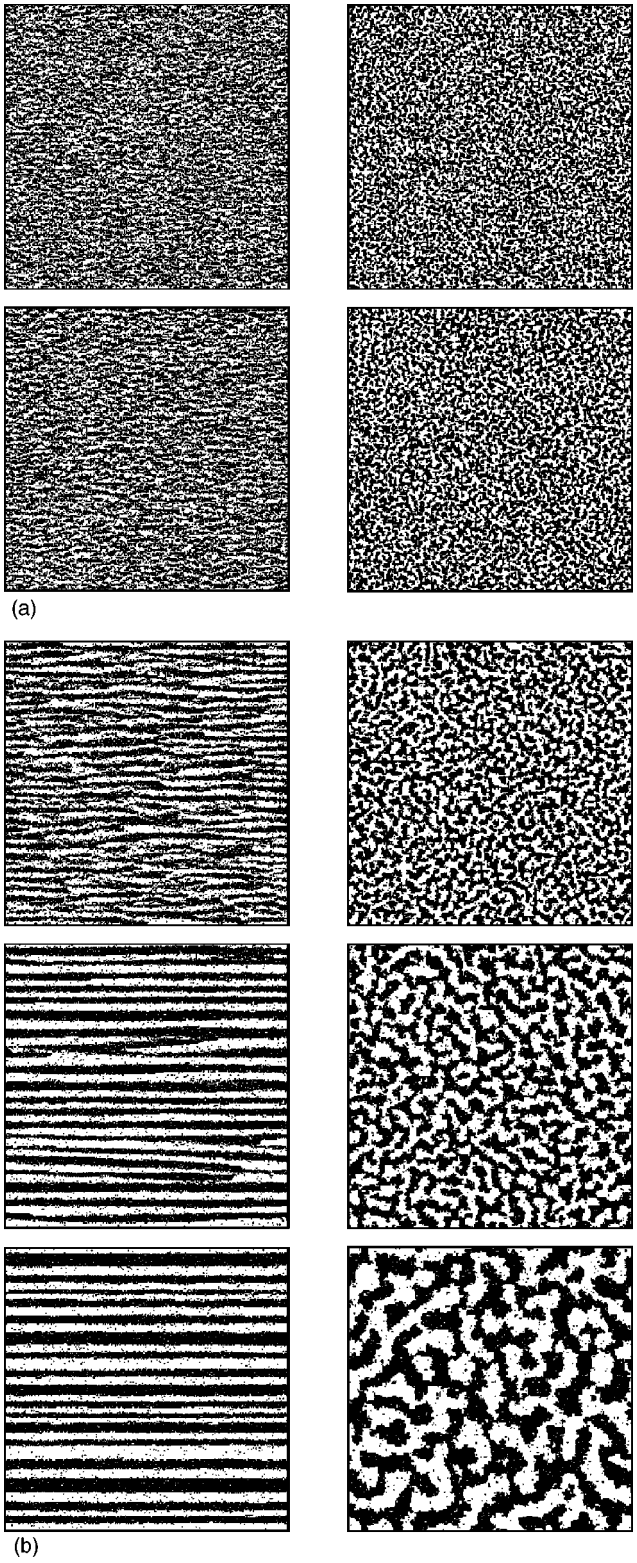

FIG. 1. (a) A series of MC snapshots comparing very early patterns for the DLG (with an infinite horizontal field) and for the standard lattice gas, i.e., zero field (LG) at the same time. This corresponds to a 256×256 lattice at $T\simeq0.6T_C^{\infty}$. The time (in MC steps) is here $t=$ 4 and 10 (from top to bottom) for the DLG (left column) and for the LG (right column). (b) The same as (a) but at late time, namely, $t=100$, 1000, and 10 000 (from top to bottom) for the DLG (left column) and for the LG (right column).

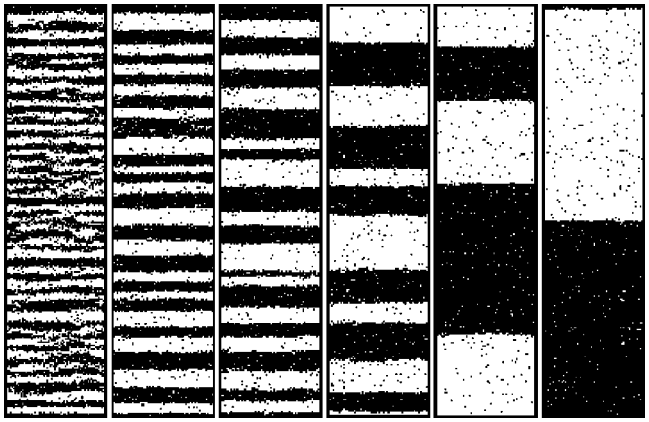

FIG. 2. A series of MC snapshots that illustrate (late) growth at $T\simeq0.6T_C^{\infty}$. This is for a rectangular lattice of size $L_{\perp}\times L_{\parallel}=256\times64$ and $t=10^2$, 10^4, 10^5, 10^6, 10^7, and 1.1×10^8 MC steps, respectively, from left to right.

Fig. 2. We notice that coalescence implies evaporation of the gas stripe between the two involved liquid stripes. Therefore, given the particle/hole symmetry, our assumption is in a sense equivalent to assuming that growth is due to evaporation of stripes;[26] however, the view adopted here allows for a more detailed description below.

In order to evaluate the implications of stripe effective diffusion via monomer events, let's assume that stripes are well defined and compact and exhibit a (linear) interface which is rather flat. This is perfectly justified at sufficiently low temperature (the case analyzed in detail here),[21] and it might hold more generally, in a wide region including the center of the miscibility gap but excluding the critical region. Under this assumption, consider a stripe of mean width $\ell(t)$ that consists of M particles whose coordinates along the transverse (vertical) direction are $y_j(t)$; $j=1,\ldots,M$. We characterize the stripe position by its center of masses, $Y_{\text{c.m.}}(t)\equiv M^{-1}\Sigma_j y_j(t)$.

Let us evaluate the mobility coefficient $\mathcal{D}_l \equiv N_{\text{me}}\langle(\Delta Y_{\text{c.m.}})^2\rangle$ which depends on the stripe width $\ell(t)$. Here N_{me} is the number of monomer events per unit time, and $\langle(\Delta Y_{\text{c.m.}})^2\rangle$ is the mean-squared displacement of the stripe associated to one of the monomer events. We think of two possible types of events, each giving a different contribution to $\mathcal{D}_l$:

(A) Evaporation condensation of particles and holes in the stripe surface. Here particles (holes) at the stripe interface evaporate to the hole (particle) gas, and condensate later at the same interface. The evolution of the evaporated particle (hole) in the bulk can be seen as a one-dimensional random walk with two absorbing walls, the left and right interfaces, respectively. According to standard random-walk theory,[34] the evaporated particle (hole) will go again with unit probability to one of the (two) possible interfaces. Moreover, the random walker will stick again to its original interface with high probability, so trapping a particle (hole) from the opposite interface is unlikely. Consequently, in this case (A), N_{me} is simply the evaporation rate. That is, $N_{\text{me,A}}=\nu\Sigma_j'\exp(-2T^{-1}\Delta_j)$ where ν is the *a priori* frequency, the sum is over the surface particles, and Δ_j is the number of

resulting broken bonds. For a flat linear interface, particles can only jump transversely away the surface, ν equals the inverse of the lattice coordination number q, and one may write $N_{\mathrm{me,A}} \approx 4q^{-1}L_{\parallel}\exp(-2\bar{\Delta}/T)$ where $\bar{\Delta}$ is the mean number of broken bonds per evaporation event. We multiplied here by 2 to take into account evaporation of surface holes that travel within the stripe to reach the (same) surface again. On the other hand, evaporation processes induce changes $\Delta Y_{\mathrm{c.m.}} = M^{-1}\delta y$, where δy is the net particle (transverse) displacement, and $M \approx L_{\parallel} \times \ell(t)$ for compact stripes. Therefore,

$$\mathcal{D}_{\ell}^{(\mathrm{A})} \sim 4q^{-1}\langle \delta y^2 \rangle e^{-2\bar{\Delta}/T} L_{\parallel}^{-1} \ell^{-2}. \tag{2}$$

(B) A hole jumps one lattice spacing away within the stripe interior. This induces $\Delta Y_{\mathrm{c.m.}} = 1/M$ or 0, depending on the jump direction. One may write $N_{\mathrm{me,B}} = 2\nu\rho_h(T) L_{\parallel}\ell p_h(T)$ where ρ_h is the density of holes, $L_{\parallel}\ell$ is the volume or total number of sites within the liquid stripe, and p_h is the jumping probability per unit time. The factor 2 here comes from the fact that a hole modifies $Y_{\mathrm{c.m.}}$ when jumping to any of the two directions $\pm\vec{y}$. At low T, ρ_h is small; holes are then rather isolated from each other, so that jumps do not modify the number of broken bonds, and $p_h \approx 1$. What ensues is

$$\mathcal{D}_{\ell}^{(\mathrm{B})} \sim 2q^{-1}\rho_h L_{\parallel}^{-1}\ell^{-1}. \tag{3}$$

Note that a different dependence of Eqs. (2) and (3) on ℓ is a consequence of the fact that the rates $N_{\mathrm{me,A}}$ and $N_{\mathrm{me,B}}$ involve processes consisting of evaporation on the line and difussion on the bulk, respectively.

For $\rho = \frac{1}{2}$, one has on the average stripes of width ℓ that are separated a distance ℓ from each other. Therefore, a given stripe takes a mean time $\tau_l = \ell^2/\mathcal{D}_{\ell}$ to find (and thus to coalesce with) another one, and this causes its width to increase by $\Delta\ell = \ell$. Consequently, $d\ell/dt \sim \Delta l \tau_{\ell}^{-1} = \mathcal{D}_{\ell}\ell^{-1}$. Together with Eqs. (2) and (3), respectively, this implies that mechanism (A) is characterized by a power law $\ell \sim t^{1/4}$, and that mechanism (B) is to be associated with $\ell \sim t^{1/3}$. Furthermore, assuming that pattern growth in the DLG is the result of competition between the two mechanisms, and that they are independent of each other, $\mathcal{D}_{\ell} = \mathcal{D}_{\ell}^{(\mathrm{A})} + \mathcal{D}_{\ell}^{(\mathrm{B})}$, it follows that

$$\frac{d\ell}{dt} \sim \frac{1}{L_{\parallel}}\left(\frac{\alpha_{\mathrm{A}}}{\ell^3} + \frac{\alpha_{\mathrm{B}}}{\ell^2}\right), \tag{4}$$

where $\alpha_{\mathrm{A}} = 4\nu\langle \delta y^2 \rangle e^{-2\bar{\Delta}/T}$ and $\alpha_{\mathrm{B}} = 2\nu\rho_h$. This is our general result for the DLG as far as the field E is large, e.g., infinite, and the temperature T is low enough so that the interfaces, and mechanisms (A) and (B), are sufficiently simple as assumed. This is to be compared with the Lifshitz-Slyozov-Wagner behavior $d\ell/dt \sim \ell^{-2}$ which assumes spatial isotropy and diffusion directly governed by surface tension. Formally, Eq. (4) is similar to an equation obtained before by assuming isotropic conditions; see Sec. I.[12]

The consequences of Eqs. (2)–(4) are as follows. Both Eqs. (2) and (3) imply independently that

$$\ell \sim (\varphi\theta)^{1/\varphi}(t/L_{\parallel})^{1/\varphi}. \tag{5}$$

The difference is that $\theta = \alpha_{\mathrm{A}}$ and $\varphi = 4$ from Eq. (2) while one obtains $\theta = \alpha_{\mathrm{B}}$ and $\varphi = 3$ from Eq. (3). On the other hand, for sufficiently late times, ℓ becomes large and Eq. (4) simply solves into

$$\ell(t) \sim \alpha t^{1/3} + \zeta, \tag{6}$$

where $\alpha^3 = 3\alpha_{\mathrm{B}}L_{\parallel}^{-1}$ and $\zeta = \alpha_{\mathrm{A}}/2\alpha_{\mathrm{B}}$. That is, the prediction is that hole diffusion within the stripe [mechanism (B)] will be dominant at late times. A different hypothesis, based on the stripe evaporation picture, was shown in Ref. 26 to imply $\ell \sim (t/L_{\parallel})^{1/3}$. This coincidence is not surprising since, as argued above, the coalescence of two particles' stripes implies the evaporation of the intermediate hole stripe and due to the particle/hole symmetry in our system, both mechanisms (stripe diffusion/coalescence and stripe evaporation) correspond to the same physical process yielding the same behavior. In order to uncover the close analogy between the two pictures, one may notice that, to evaporate a particle stripe, many of its particles must cross the surrounding hole stripes and stick to the neighboring particle stripes (this is so since the particle density in the gas phase remains almost constant). This particle migration process through the surrounding hole stripes is in fact what we have called ''hole diffusion within the stripe'' in the presence of particle/hole symmetry. Hence the fundamental mechanism involved in a stripe evaporation is the diffusion of its constituents through the neighboring stripes. This observation is key to understanding the relation between the stripe's evaporation and hole (particle) diffusion.

The effect of mechanism (A)—surface evaporation and subsequent condensation—on growth is more subtle. In fact, our theory predicts a crossover from the $t^{1/4}$ regime to the $t^{1/3}$ regime as time is increased. That is, the two mechanisms will have a comparable influence at $t \sim \tau_{\mathrm{cross}}$ with

$$\tau_{\mathrm{cross}} = \frac{(4\alpha_{\mathrm{A}})^3}{(3\alpha_{\mathrm{B}})^4} L_{\parallel}. \tag{7}$$

For times $t < \tau_{\mathrm{cross}}$, mechanism (A) is dominant and the $t^{1/4}$ behavior is expected, while mechanism (B) is dominant for $t > \tau_{\mathrm{cross}}$ and the asymptotic $t^{1/3}$ growth law is then observed. The crossover time τ_{cross} is a macroscopic, observable time. Further, we may define the time τ_{ss} at which a single stripe is reached by the condition that $\ell(t) \approx \frac{1}{2}L_{\perp}$. One obtains

$$\tau_{\mathrm{ss}} = \frac{L_{\parallel}}{\alpha_{\mathrm{B}}}\left\{\frac{L_{\perp}^3}{24} - \frac{\zeta L_{\perp}^2}{4} + 2\zeta^2 L_{\perp} - 8\zeta^3\left[\ln\frac{\alpha_{\mathrm{B}}(2\zeta + 1/2L_{\perp})}{L_{\parallel}} - \ln\frac{2\zeta\alpha_{\mathrm{B}}}{L_{\parallel}}\right]\right\}. \tag{8}$$

Hence our system is characterized by two different time scales, namely, τ_{cross} and τ_{ss}. They depend on system size in a different way. For large systems one generally obtains $\tau_{\mathrm{ss}} \gg \tau_{\mathrm{cross}}$, so that the system converges, after a short, perhaps unobservable transient time, to the relevant $t^{1/3}$ behavior. However, there are small systems for which $\tau_{\mathrm{ss}} < \tau_{\mathrm{cross}}$. These systems will reach the stationary state (a single stripe) before having time to enter into the asymptotic $t^{1/3}$ regime.

For these small systems, the only relevant behavior is the $t^{1/4}$ one. Therefore, there is a *size* crossover between $t^{1/4}$ asymptotic behavior for small systems and $t^{1/3}$ asymptotic behavior for large ones. The condition $\tau_{\rm cross}(T,L_\parallel) = \tau_{\rm ss}(T,L_\parallel,L_\perp)$ defines the crossover size.

Consider now the parameter $\gamma \equiv \tau_{\rm cross}(T,L_\parallel)/\tau_{\rm ss}(T,L_\perp,L_\parallel)$. It follows that the $t^{1/3}$ behavior is dominant for $\gamma \ll 1$. However, one also has that $\gamma(T,L_\perp,L_\parallel)\to 0$ for finite T in the thermodynamic limit ($L_\perp,L_\parallel\to\infty, L_\perp/L_\parallel = {\rm const}$). Consequently, the $t^{1/3}$ growth law is the general one, namely, the only one we should expect to observe in a macroscopic system. Corrections to this should only occur at early times in small systems. This is fully confirmed below.

One may also define a longitudinal length,[26,27] say, $l_\parallel \sim t^{a_\parallel}$, where one expects $a_\parallel > 1/3$ (given that the growth is more rapid longitudinally than transversely). This length is only relevant during the initial regime, until stripes become well defined, with all of them extending the whole length of $L_\parallel$. This condition may be taken as defining the onset of the multistripe state, which may be characterized by $l_\parallel(\tau_{\rm ms}) = L_\parallel$, from where it follows that $\tau_{\rm ms}\sim L_\parallel^{1/a_\parallel}$. Interesting enough, this is on the macroscopic time scale, as for both $\tau_{\rm cross}$ and $\tau_{\rm ss}$ (more precisely, $\tau_{\rm cross}\sim L_\parallel$ and $\tau_{\rm ss}\sim L_\parallel L_\perp^3$). The fact that all these relevant times are on the macroscopic, observable time scale confirms that, as argued above, the single-stripe (and not the multistripe) state is the only stable one in general. It is also to be remarked that, once the multistripe state sets in, the only relevant length is the transverse one, l. Of course, this is compatible with the possible existence of two correlation lengths describing thermal fluctuations at criticality.

In order to test our predictions, several measures of the relevant length in computer simulations were monitored, namely,

(i) the maximum width of the stripe, $\ell_{\rm max}$, averaged over all stripes in the configuration. This maximun width is defined as the distance in the direction perpendicular to the field between the leftmost and the rightmost particles within the stripe;

(ii) $\ell_M \equiv M/L_\parallel$, where $M = M(t)$ is the mass, or number of particles belonging to the stripe, averaged over all stripes in the configuration. This mass width is defined as the width of a perfectly dense stripe with M particles;

(iii) $\ell_s \equiv L_\perp/2N_s$, where N_s is the number of stripes in the configuration.

After averaging over many independent evolutions, all these quantities happen to behave similarly with time. Further measures of the relevant length that we define in the next section behave in the same way. We shall refer to this common behavior, which is illustrated in Fig. 3, as $\ell(t)$. [It is noticeable that, before showing a common behavior, Fig. 3 reveals some significant differences between our measures of $\ell(t)$ at early times. This confirms the more difficult description—not attempted here—which is required by the initial regime.]

In Fig. 4 we illustrate our analysis and main results concerning the (late) time evolution of $\ell(t)$. The predictions above are confirmed and, in particular, "small" lattices—

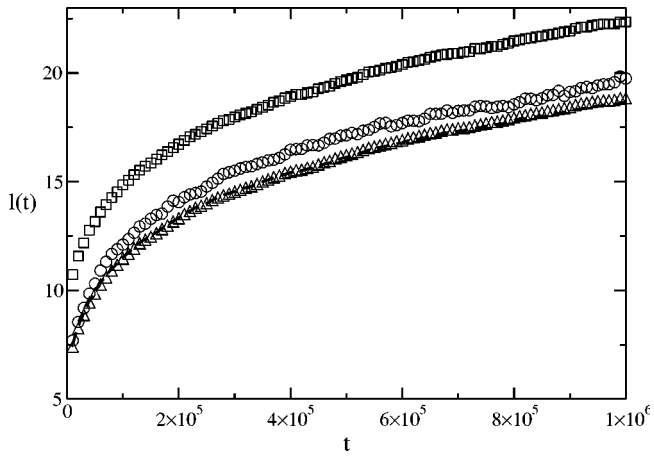

FIG. 3. Time evolution of the relevant length, $\ell(t)$, as obtained by different methods, namely, from the number N_s of stripes (dashed line), from the maximum width $\ell_{\rm max}$(squares) from the mass ℓ_M(triangles), and from the peak of the structure function, $\ell_S \equiv 2\pi/k_{\perp,{\rm max}}$(circles); these quantities are defined in the main text. The graphs here correspond to an average of over 600 independent runs for the 128×128 lattice.

Fig. 4(a)—happen to behave differently than "large" lattices—Fig. 4(b). In both cases we plotted $\ell(t)$ versus $t^{a_\perp}$ for varying $a_\perp$, looking for the best linear fit $\ell(t) = \alpha t^{a_\perp} + \zeta$, excluding the initial time regime. The upper insets in the figures show the chi square function associated to each fit, namely,

$$\chi^2(a_\perp) = \sum_{i=1}^{\eta} \frac{[\ell(t_i) - (\alpha t_i^{a_\perp} + \zeta)]^2}{\alpha t_i^{a_\perp} + \zeta}, \tag{9}$$

for a least-squares fit to η data points using parameters $a_\perp$, α, and ζ. The main graphs confirm the existence of a common behavior for all the monitored measures of $\ell(t)$ (indicated by different symbols). These graphs also demonstrate that $\ell(t) = \alpha t^{a_\perp} + \zeta$, with small ζ, during the whole time regime of consideration. On the other hand, the upper insets indicate that $a_\perp$ is very close to $\frac{1}{4}$ for "small" systems (in fact, for $L_\perp \leqslant 128$) while $a_\perp \simeq \frac{1}{3}$, as the system becomes larger, say, $L_\perp \geqslant 256$, corresponds to a "large" lattice according to familiar MC standards. As an alternative method to analyze $\ell(t)$, one may evaluate

$$\overline{a}(t) \equiv \frac{d\log_n \ell(t)}{d\log_n t}. \tag{10}$$

Our prediction is that $\overline{a}(t) = a_\perp - \zeta a_\perp/\ell(t)$, i.e., this should provide the exponent $a_\perp$ by extrapolating to large $\ell(t)$ (late time). The insets at the bottom of Figs. 4(a) and 4(b) show the results for $n=2$. They are in agreement with the other method, and again confirm our predictions.

As indicated above, the size crossover between the $t^{1/4}$ and $t^{1/3}$ asymptotic regimes is expected for a system size $(L_\parallel, L_\perp)$ such that $\tau_{\rm cross}(T,L_\parallel) = \tau_{\rm ss}(T,L_\perp,L_\parallel)$. In order to make this condition explicit, we need to estimate the amplitudes $\alpha_{\rm A}$ and $\alpha_{\rm B}$ in Eq. (4); see Eqs. (7) and (8). These

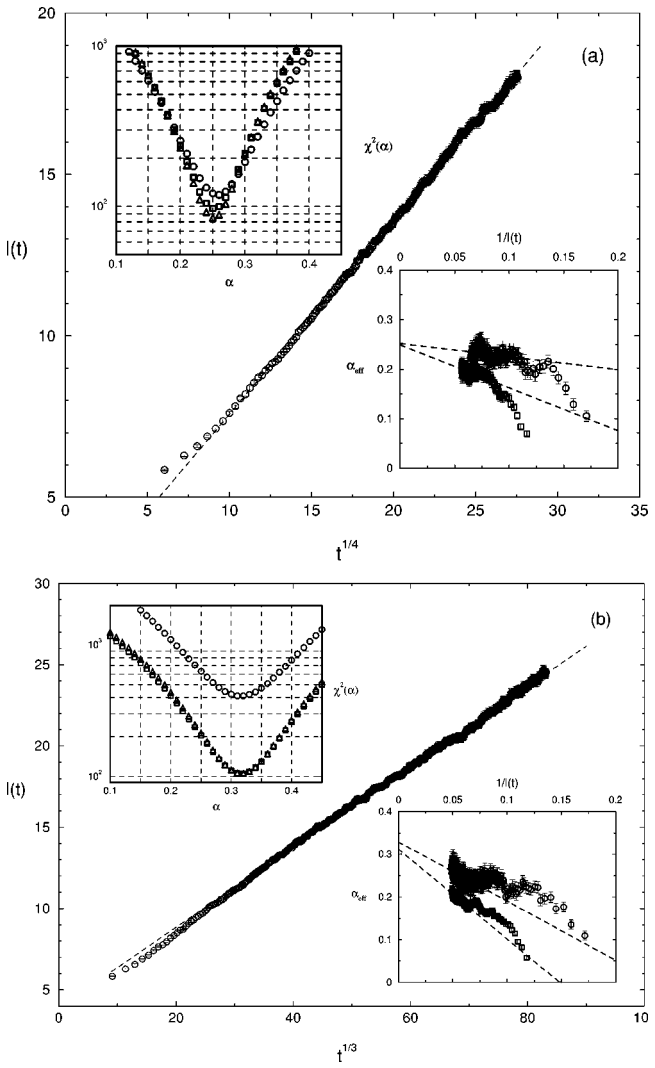

FIG. 4. (a) The main graph shows $\ell(t)=\ell_S(t)$ versus $t^{a_\perp}$ for $a_\perp=\frac{1}{4}$ in the case of the ''small'' 64×64 lattice. A similar behavior is obtained for any of the studied measures of ℓ (see the main text for definitions), which are represented in the insets by different symbols, namely, $\ell_{\max}$ (squares), ℓ_S (circles), and ℓ_M (triangles). The upper inset shows the chi square function for varying $a_\perp$ as obtained from a series of fits; a well-defined minimum is exhibited indicating that $a_\perp\simeq\frac{1}{4}$ in this case. The lower inset shows the *effective exponent*, $d\log_2\ell/d\log_2 t$, as a function of $1/\ell(t)$; this extrapolates to the same value of $a_\perp$. Same as (a) but demonstrating that $a_\perp=\frac{1}{3}$ for the ''large'' $L_\perp\times L_\parallel=256\times64$ lattice (one obtains a similar result for larger $L_\parallel$).

amplitudes, which state the relative importance of surface evaporation/condensation versus bulk hole diffusion, are given, respectively, by $\alpha_{\rm A}=4q^{-1}\langle\delta y^2\rangle e^{-2\bar{\Delta}/T}$ and $\alpha_{\rm B}=2q^{-1}\rho_h$. We note that, for a sufficiently flat interface (i.e., one that involves microscopic—but not macroscopic—roughness), $\langle\delta y^2\rangle\sim\mathcal{O}(1)$ and $\bar{\Delta}\simeq5$. On the other hand, the excess energy associated with an isolated hole is 16, so that $\rho_h\sim\exp(-16/T)$ is a rough estimate of the hole density. As depicted in Fig. 5, it follows numerically, in full agreement with our observations, that $a_\perp=\frac{1}{4}$ is to be observed only at early times, earlier for larger systems; to be more specific,

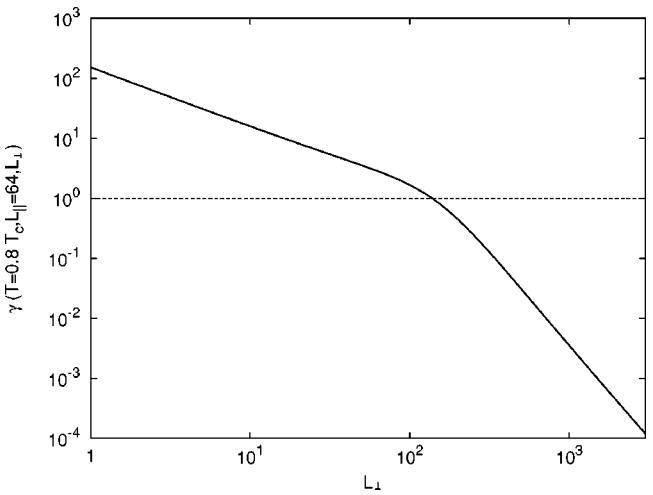

FIG. 5. The parameter $\gamma=\tau_{\rm cross}(T,L_\parallel)/\tau_{\rm ss}(T,L_\perp,L_\parallel)$, with the characteristic times $\tau_{\rm cross}$ and $\tau_{\rm ss}$ defined in the main text, as a function of $L_\perp$ for $L_\parallel=64$. This confirms our distinction between ''small'' and ''large'' lattices, as explained in the main text.

the crossover for $L_\parallel=64$, for instance, is predicted for $L_\perp\sim140$, which confirms the above; see also Figs. 4(a) and 4(b).

This behavior may be understood on simple grounds. The surface/volume ratio is large initially and, consequently, mechanism (A) (based on surface events) is then dominant. This is more dramatic the smaller the system. That is, the surface is negligible for macroscopic systems, in general, and, as illustrated in Fig. 2, even if the surface is relevant at very early times, its ratio to the volume will monotonically decrease with time. This causes hole diffusion in the bulk [mechanism (B)] to become dominant, more rapidly for larger systems, since the liquid phase is trying to exhibit only two surfaces. On the other hand, Ref. 26 studies the stripe coarsening process in the infinitely driven lattice gas. Pure $t^{1/3}$ behavior is reported assuming the stripe evaporation mechanism. This result is perfectly compatible with our results, given that the systems in Ref. 26 correspond to very large values of $L_\perp$ (800 and 960) and small values of $L_\parallel$ (8, 16, and 32). For these shapes our theory also predicts the (simple) $t^{1/3}$ asymptotic behavior.

IV. CORRELATIONS AND THE STRUCTURE FACTOR

Consider now the Fourier transform of the pair-correlation function $C(x,y;t)=\langle n_{0,0}(t)n_{x,y}(t)\rangle$ where $n_{x,y}$ stands for the occupation variable at lattice site $\vec{r}=(x,y)$. This is the so-called structure factor, $S(\vec{k},t)$, where $\vec{k}=(k_\parallel,k_\perp)$. Given that the $k_\parallel$ dependence is only relevant at early times, before the multistripe state sets in, i.e., for $t<\tau_{\rm ms}$, we shall set $k_\parallel=0$ in the following. That is, our interest here is on

$$S(k_\perp;t)=\frac{1}{L_\parallel L_\perp}\left|\sum_{x,y}n_{x,y}(t)\exp[ik_\perp y]\right|^2. \qquad (11)$$

As illustrated in Fig. 6, this function develops a peak at $k_\perp=k_{\max}(t)$ immediately after quenching. The peak then mono-

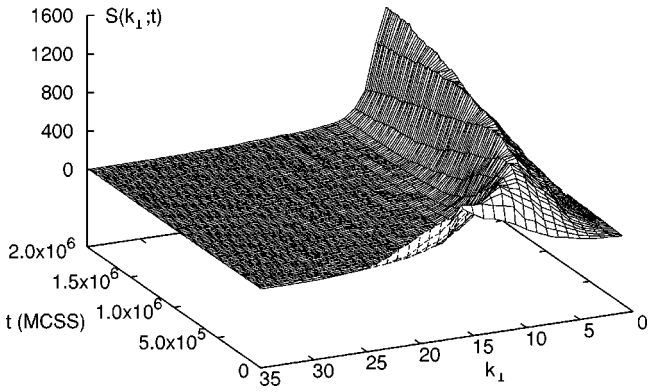

FIG. 6. Time development of the structure factor $S(k_\perp;t)$, as defined in the main text, for a "large" lattice $L_\perp \times L_\parallel = 256 \times 256$ during early and intermediate phase segregation. A peak grows with time as it shifts towards the small values of $k_\perp$.

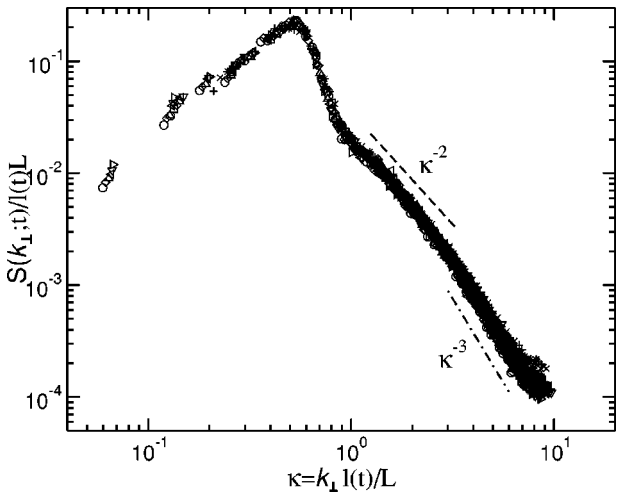

FIG. 7. The scaling with both time and size of the structure function to show that $\Phi(\varkappa) \equiv S(k_\perp;t)/lL$, with $\varkappa = k_\perp l L^{-1}$, is well defined and universal, i.e., the same at any time (excluding some early evolution) and for any square lattice of side L. This plot includes all data for $t \geqslant 10^4$ MC steps and 64×64, 128×128, and 256×256 lattices. The broken lines illustrate the different kinds of behavior of $\Phi(\varkappa t)$ that are discussed in the main text.

tonically shifts towards smaller wave numbers with increasing t; in fact, one expects $k_\perp \to 0$ as $t \to \infty$ in a macroscopic system. The wavelength $\ell_S \equiv 2\pi/k_{\max}$ turns out to be an excellent characterization of the relevant order, namely, it measures both the stripe width and the stripe separation during phase segregation. In particular, we confirm that $\ell_S(t)$ has the common behavior discussed above for length $\ell(t)$; see Figs. 3 and 4.

The fact that the DLG shows a unique *time-dependent* relevant length, $\ell_\perp = l(t)$, has some important consequences. For example, extrapolating from the equilibrium case (see Sec. I),[7] one should probably expect dynamical scaling, i.e.,

$$S(k_\perp;t) \propto l(t) F[k_\perp l(t)] \tag{12}$$

for the anisotropic DLG in two dimensions. This is indeed observed to hold during most of the relaxation and, in particular, during all of the segregation process after formation of well-defined stripes. This is illustrated in Fig. 7 depicting the scaling function F. A time-dependent mean-field model of a binary mixture in shear flow has recently been demonstrated to exhibit a similar property, though involving two lengths both behaving differently from $\ell(t)$ above.[18]

The structure factor may be obtained by scattering, which makes it an important tool in many studies. Analyzing further the details of functions $S(k_\perp;t)$ and $F(\varkappa)$ or, alternatively, the universal function $\Phi(\varkappa) \equiv S/\ell L$, as observed in computer simulations is therefore of great interest [the extra L factor in the definition of $\Phi(\varkappa)$ is our finite-size scaling ansatz]. Experimental studies often refer to the mean "radius of gyration" of the grains as the slope of the straight portion in a plot of $\ln[S(k,t)]$ versus k^2.[35] We checked the validity under anisotropic conditions of this concept, which is in fact quite useful in equilibrium even outside the domain of validity of its approximations.[7] We confirm that $S(k_\perp;t)$ exhibits the Guinier Gaussian peak, namely,

$$\Phi(\varkappa) \sim \exp[-\text{const}(\varkappa - \varkappa_{\max})^2] \tag{13}$$

around the maximum $\varkappa_{\max}$. More intriguing is the behavior of $\Phi(\varkappa)$ before the peak, $\varkappa < \varkappa_{\max}$. Figure 7 indicates that scaling does not hold in this region even at the end of our (otherwise long enough) simulations. This is so because $\Phi(\varkappa)$ goes as $\rho^2 L/\ell(t)$ at $k_\perp = 0$, and thus depends on time for very small values of $\varkappa$, breaking the scaling observed for larger values of $\varkappa$. However, a detailed study of data reveals that the scaling function near the origin tends with time towards a common envelope $\Phi(\varkappa) \sim \varkappa^{1+1/3}$ for $\varkappa_0 < \varkappa < \varkappa_{\max}$; we do not have a simple explanation of this. In any case, this behavior breaks down close to the origin, $\varkappa \lesssim \varkappa_0$, where $\Phi(\varkappa) \to 0$ as $\varkappa \to 0$ and $t \to \infty$ for the infinite system.

The behavior after the peak, $\varkappa > \varkappa_{\max}$, may be predicted on simple grounds. The (sphericalized) structure factor for (equilibrium) isotropic binary mixtures is known to satisfy the Porod law, $S \sim k^{-(d+1)}$ at large enough k, where d is the system dimension,[7] i.e., $S \sim k^{-3}$ in two dimensions. The main contribution to the large-k tail comes from the short-distance behavior of $C(x,y;t)$. That is, the Porod's region for the DLG may be taken to correspond to $\lambda_\perp \ll k_\perp^{-1} \ll \ell(t)$ where $\lambda_\perp$ stands for a (transverse) thermal length that characterizes the smallest, thermal fluctuations. Let two points, $\vec{r}_0$ and $\vec{r}_0 + \vec{r}$, $\vec{r} = (x,y)$. For any x such that $\lambda_\perp \ll x \ll \ell(t)$, one roughly has that the product $n_{\vec{r}_0}(t) n_{\vec{r}}(t)$ equals $+1$ if the two points are on the stripe, and 0 otherwise, i.e., if either an interface exists between them or else the two points belong to the gas between stripes. Since $x \ll \ell(t)$, the probability that $\vec{r}$ crosses more than one interface is negligible. For a half filled system, the probability that $\vec{r}_0$ lies at a particle stripe is $\frac{1}{2}$, and the probability that both $\vec{r}_0$ and $\vec{r}_0 + \vec{r}$ belong to the same stripe is roughly $\frac{1}{2}[\ell(t) - x]/\ell(t)$. Hence,

$$C(x,y;t) \simeq \frac{1}{2}\left(1 - \frac{x}{l(t)}\right), \quad x \ll \ell(t). \tag{14}$$

By power counting, this implies the *anisotropic* Porod law (in two dimensions)

$$S(k_\perp;t)\sim\frac{1}{\ell(t)k_\perp^2},\quad \lambda_\perp\ll k_\perp^{-1}\ll l(t). \tag{15}$$

Therefore, $\Phi(\varkappa)\sim\varkappa^{-2}L^{-1}$, which is confirmed in Fig. 7. This is in contrast with the (isotropic) Porod result. The difference is a consequence of the fact that the DLG clusters are stripes that percolate in the direction of the field, instead of the isotropic clusters of the LG. The short-distance pair-correlation function for the latter is $C(\vec{r};t)\simeq\frac{1}{2}[1-|r|/\ell(t)]$, from which one has that $\Phi(\varkappa)\sim\varkappa^{-3}$. It follows that anisotropy may easily be detected by looking at the tail of the structure factor.

The detailed analysis of $S(k_\perp;t)$ also reveals that, as $L_\parallel$ is increased in computer simulations, the anisotropic behavior $\Phi\sim\varkappa^{-2}$ crosses over to $\Phi\sim\varkappa^{-3}$ for larger $\varkappa$; see Fig. 7. We believe this reflects the existence of standard thermal fluctuations. That is, very small clusters of particles occur in the gas in the asymptotic regime whose typical size in the direction perpendicular to the field is of order $\lambda_\perp$. These very small asymptotic clusters are rather isotropic, namely, they do not differ essentially from the corresponding ones in equilibrium binary mixtures. More specifically, for $x\sim\lambda_\perp$, one may approximate $C(\vec{r};t)\sim 1-|r|/\lambda_\perp(t)$, which implies the $\varkappa^{-3}$ power-law tail for large $\varkappa$. On the other hand, according to (5), the mean stripe width grows as $\ell(t)\sim(t/L_\parallel)^a$ with $a=\frac{1}{4}$ or $a=\frac{1}{3}$, depending on the value of $L_\perp$. Therefore, the number of stripes at time t is proportional to $L_\perp L_\parallel^a/t^a$ and, for a given time, the number of stripes increases with $L_\parallel$ as $L_\parallel^a$. We also know that, at a given time, the number of small, fluctuating clusters is proportional to $L_\parallel$. Hence the relative importance of small clusters due to thermal fluctuations as compared to stripes is proportional to $L_\parallel$. In fact, the $\varkappa^{-3}$ tail is observed for large enough values of $L_\parallel$ but not for small lattices.

V. A CONTINUUM DESCRIPTION

The rigorous derivation of a general continuum analog of the driven lattice gas is an open problem.[21] Recent studies led to the following proposal for a coarse-grained density, $\phi(\mathbf{r},t)$:[36,37]

$$\partial_t\phi(\mathbf{r},t)=\tau_\perp\nabla_\perp^2\phi-\nabla_\perp^4\phi+\frac{\lambda}{6}\nabla_\perp^2\phi^3+\tau_\parallel\nabla_\parallel^2\phi+\nabla_\perp\xi(\mathbf{r},t). \tag{16}$$

Here, the last term stands for a conserved Gaussian noise representing the fast degrees of freedom, and $\tau_\perp$, $\tau_\parallel$, and λ are model parameters. Compared to previous proposals,[24,38] this Langevin-type equation amounts to neglect a nonlinear current term, $-\alpha\nabla_\parallel\phi^2$, that was believed to be essential (*relevant*) at criticality. However, one may show that, at least in the limit $E\to\infty$, the coefficient α cancels out (due in this case to a subtle saturation effect).[37] In fact, recent scaling analysis has unambiguously confirmed that a particle current is not relevant and that Eq. (16) captures the correct critical behavior of the DLG.[27,28] Consequently, an important question is now whether Eq. (16) reproduces also the kinetic behavior of the DLG as described in previous sections. We present in this paper a confirmation that, as compared with other approaches,[24] Eq. (16) is indeed a proper continuum description of the DLG kinetic relaxation. A more complete study of the kinetic consequences of this equation will be presented elsewhere.

In order to numerically integrate Eq. (16), let us introduce the indices $i,j=1,\ldots,N$ to represent, respectively, the two components of $\mathbf{r}\equiv(x_\perp,x_\parallel)$. One thus makes a trivial discretization of the space, and then of the time by the Cauchy-Euler method.[39] The result is a set of N^2-1 coupled nonlinear equations, namely,

$$\phi(i,j;t+\Delta t)=\phi(i,j,t)+\Delta t\Big[\tau_\perp\tilde{\nabla}_\perp^2\phi-\tilde{\nabla}_\perp^4\phi+\frac{\lambda}{6}\tilde{\nabla}_\perp^2\phi^3+\tau_\parallel\tilde{\nabla}_\parallel^2\phi\Big]+\sqrt{\Delta t}\tilde{\nabla}_\perp\xi(i,j;t). \tag{17}$$

This equation is to be solved by the computer. With this aim, we may write $\tilde{\nabla}_\perp\xi(i,j;t)=[\xi(i+1,j;t)-\xi(i-1,j;t)]/2\Delta x_\perp$ and $\phi(i,j;t)\equiv\phi(i\Delta x_\perp,j\Delta x_\parallel;t)$ where $\Delta x_\perp=L_\perp/N$ and $\Delta x_\parallel=L_\parallel/N$. The maximum value of $\Delta x_\perp$ is thus limited by the interface width. For Fig. 8, which concerns a 256×256 lattice ($N=256$) we—rather arbitrarily—used $\Delta x_\perp=\Delta x_\parallel=1.7$, and $\Delta t=0.05$, which produce a locally stable solution. The parameters $\tau_\perp$, $\tau_\parallel$, and λ are fixed on the basis of its physical meaning. The mass terms $\tau_\parallel$ and $\tau_\perp$ represent temperatures along the longitudinal and transverse directions, respectively, relative to the critical temperature, i.e., $\tau_\perp\sim(T_\perp-T_C^\infty)$. Given the anisotropy of phase segregation, with longitudinal interfaces only, $\tau_\perp<0$ and $\tau_\parallel>0$. On the other hand, $|\tau_\perp|$ should be small enough to allow for a relatively fast evolution. Our choices for Fig. 8 are $\tau_\perp=-0.25$, $\tau_\parallel=0.5$, and $\lambda=1$.

It is remarkable that, in spite of some apparent similarity, the problem here differs from the one in the study of (standard) spinodal decomposition by means of the isotropic ($E=0$) Cahn-Hilliard equation. In equilibrium,[40] one usually assumes that the influence of noise on growth, which is then assumed to be directly driven by surface tension, is negligible far from criticality. The noise term in Eq. (17) may be expected to be important in a more general context, however. That is, as described in Sec. III, the DLG develops striped patterns in which surface tension smooths the interfaces but has no other dominant role on the basic kinetic events. Consequently, neglecting the noise in Eq. (17) would turn metastable any striped geometry after coarsening of strings, which is not acceptable (see Sec. III).

Finally, it is interesting to notice that if a one-dimensional structure is assumed, and the gradient in the direction parallel to the field in Eq. (16) is eliminated, then this equation reduces to the one-dimensional time-dependent Ginzburg-Landau model in Ref. 41. There a $\ln(t)$ growth was found at zero temperature and a crossover from $\ln(t)$ to $t^{1/3}$ at finite temperatures.

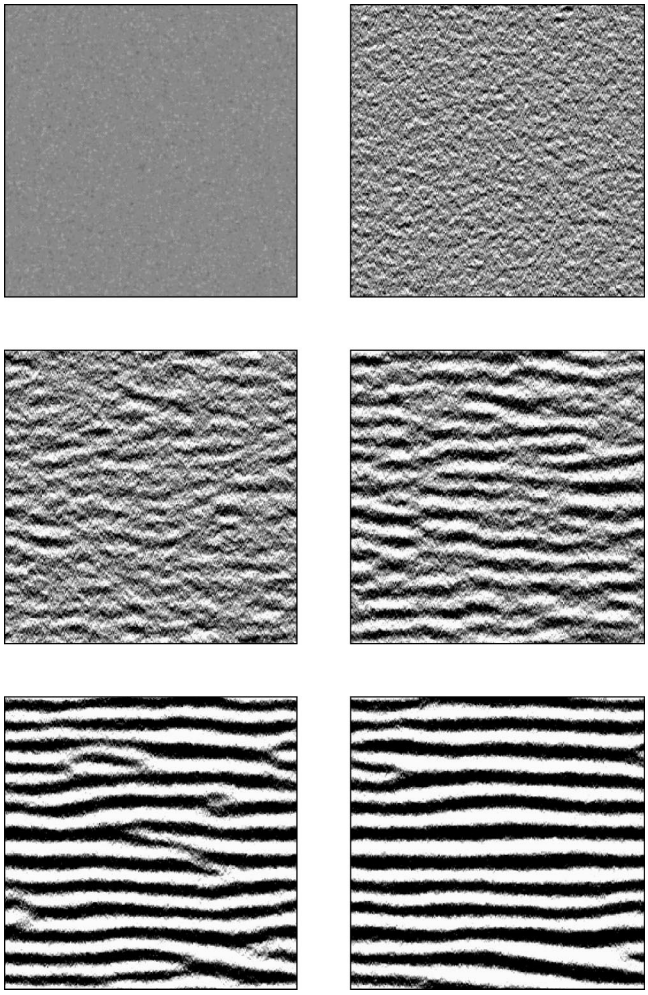

FIG. 8. Series of snapshots as obtained from Eq. (17) for the 256×256 lattice with parameters as given in the main text. Time (arbitrary units) is $t=0$, 10, 100, 200, 500, and 1000, respectively, from left to right and from top to bottom.

VI. CONCLUSION

This paper presents a theoretical description of spinodal decomposition in the DLG, and compares it with data from a kinetic Monte Carlo study. This is also compared with the kinetic implications of a Langevin, continuum equation that had previously been shown to capture correctly the critical behavior of the DLG. The resulting picture from these three approaches, which is summarized below, should probably hold for a class of highly-anisotropic phase segregation phenomena. In fact, our results provide a method for analyzing experiments that could be checked against laboratory realizations of the DLG, i.e., the case of phase segregation under biased fields or other influences such as electric fields, gravity, and elastic stresses.

Immediately after a deep quench, there is an early regime in which anisotropic grains develop. They tend to coarsen to form small strings that then combine into well-defined thin stripes. Such nucleation and early coarsening (Fig. 1) seem governed by surface tension at the string ends competing with other both surface and bulk processes. This complicated situation typically extends less than 10^3 MC steps in computer simulations, which corresponds to a very short macroscopic time, so that it would be hardly observable in experiments. As a matter of fact, most of the system relaxation proceeds by coarsening of stripes until full segregation (Fig. 2). Surprisingly enough, this regime, which has been studied for more than a decade now,[22–26] happens to be theoretically simpler than the corresponding one for the isotropic case.[1–11]

The evolution from many stripes to a single one mainly proceeds by competition of two mechanisms: (A) evaporation of a particle from one stripe surface and subsequent deposition at the same surface, and (B) diffusion of a hole within the bulk of the stripe. The first one dominates initially (and lasts more for smaller systems), when the surface/volume ratio is relatively large. Mechanism (A) implies that the relevant length (as defined in Fig. 3) increases with time according to $\ell(t)\sim t^{1/4}$. The surface/volume ratio decreases with time, however, and mechanism (B) soon becomes dominant. This implies $\ell(t)\sim t^{1/3}$ which is the general prediction for a macroscopic system (cf. Figs. 4 and 5).[42] This was obtained before by assuming coarsening of two (liquid) stripes by evaporation of the gas stripe placed between them;[26] see also Ref. 22. Note that the $t^{1/3}$ law is precisely the behavior which is acknowledged to be dominant under isotropy, but this has a different origin in the equilibrium case.[4,5] Note also that surface tension determines evaporation rates but has no other influence on mechanisms (A) and (B).

The $t^{1/3}$ growth law, Eq. (6), is perfectly confirmed by the DLG data [Fig. 4(b)]. This indicates time-scale invariance. In fact, such invariance was demonstrated for the isotropic case, in which the situation is somewhat more involved (Sec. I). The invariance property may be better analyzed by looking at the structure factor transversely to the drive, $S(k_\perp,t)$ (Fig. 6). This exhibits *dynamic scaling*, i.e., it remains self-similar during phase segregation.[43] More specifically, $\Phi(\varkappa)\equiv S(k_\perp;t)/\ell L$, with $\varkappa=k_\perp \ell L^{-1}$, is universal, namely, the same at any (sufficiently late) time t and for any square lattice of side L. Furthermore, the function $\Phi(\varkappa)$ has a well-defined shape. In particular, it exhibits the Guinier Gaussian peak, and this is followed by the anisotropic Porod decay, $\Phi(\varkappa)\sim\varkappa^{-2}$ and then by a thermal tail $\Phi(\varkappa)\sim\varkappa^{-3}$ (Fig. 7). Also noticeable is the fact that the parameter to scale along the S axis is $J(t)=\ell$ and not ℓ^2 as under isotropy.

Our results in this paper have two main restrictions, both due to the great computational effort required by this problem.[21] First, they follow from an extensive analysis of only one phase-diagram point, namely, $\rho=\frac{1}{2}$, $E=\infty$, and $T=0.8T_C^0$. However, our own observations (including the brief investigation of other points), together with an extrapolation of the many results known for the isotropic case, strongly suggest that the picture in this paper holds within a large domain around the center of the miscibility gap.[44] In fact, the scaled structure factor for isotropic systems was shown to be almost independent of density and temperature, and even the substance investigated, in a wide region below the coexistence line.[10] Our consideration of only a two-dimensional system does not seem to be a real restriction either. That is, adding an extra (transverse) dimension should not essentially modify the picture here.[45]

It would be interesting to look next in the laboratory for

both time scale invariance and $t^{1/3}$ growth under highly anisotropic conditions. In fact, there is some evidence of such behavior in sheared fluids (Sec. I), and one may think of some more direct experimental realizations of the driven lattice gas. In particular, coarsening striped patterns very similar to those observed in our system are found in some intriguing experiments on granular binary mixtures under shaking.[46] We think that the mechanisms we propose in this paper should help the understanding of such experimental results. In general, we hope our observations will motivate both experiments and more complete theories.

ACKNOWLEDGMENTS

We acknowledge very useful discussions with Raúl Toral and Miguel Ángel Muñoz, and support from MCYT, Project Nos. PB97-0842 and BFM2001-2841.

[1] K. Binder, M. H. Kalos, J. L. Lebowitz, and J. Marro, Adv. Colloid Interface Sci. **10**, 173 (1979); K. Binder, Rep. Prog. Phys. **50**, 783 (1987).

[2] J. D. Gunton, M. San Miguel, and P. S. Shani, in *Phase Transitions and Critical Phenomena*, edited by C. Domb and J. L. Lebowitz (Academic Press, New York, 1983), Vol. 8.

[3] H. Furukawa, Adv. Phys. **34**, 703 (1985).

[4] A. J. Bray, Adv. Phys. **43**, 357 (1994).

[5] K. Binder and P. Fratzl, *Spinodal Decomposition*, in *Phase Transformations in Materials*, edited by G. Kostorz (Wiley-VCH, Weinheim, 2001), pp. 409–480.

[6] S. K. Ma, *Statistical Mechanics* (World Scientific, Singapore, 1985).

[7] J. Marro, J. L. Lebowitz, and M. Kalos, Phys. Rev. Lett. **43**, 282 (1979); Acta Metall. **30**, 297 (1982); P. Fratzl, J. L. Lebowitz, J. Marro, and M. H. Kalos, *ibid.* **31**, 1849 (1983).

[8] J. Marro, R. Toral, and A. M. Zahra, J. Phys. C **18**, 1377 (1985).

[9] I. M. Lifshitz and V. V. Slyozov, J. Phys. Chem. Solids **19**, 35 (1961); C. Wagner, Z. Elektrochem. **65**, 58 (1961).

[10] G. F. Mazenko and R. Wickham, Phys. Rev. E **51**, 2886 (1995).

[11] R. Toral and J. Marro, Phys. Rev. Lett. **54**, 1424 (1985).

[12] D. A. Huse, Phys. Rev. B **34**, 7845 (1986).

[13] S. Puri, A. J. Bray, and J. L. Lebowitz, Phys. Rev. E **56**, 758 (1997).

[14] D. Beysens and M. Gbadamassi, Phys. Rev. A **22**, 2250 (1980).

[15] C. Chan and L. Lin, Europhys. Lett. **11**, 13 (1990).

[16] A. Onuki, J. Phys.: Condens. Matter **9**, 6119 (1997).

[17] N. P. Rapapa and A. J. Bray, Phys. Rev. Lett. **83**, 3856 (1999).

[18] F. Corberi, G. Gonnella, and A. Lamura, Phys. Rev. E **61**, 6621 (2000).

[19] B. B. Mandelbrot, *Multifractals and* $1/f$ *Noise* (Springer, New York, 1999).

[20] S. Katz, J. L. Lebowitz, and H. Spohn, J. Stat. Phys. **34**, 497 (1984).

[21] J. Marro and R. Dickman, *Nonequilibrium Phase Transitions in Lattice Models* (Cambridge University, Cambridge, England, 1999).

[22] C. Yeung, T. Rogers, A. Hernandez-Machado, and D. Jasnow, J. Stat. Phys. **66**, 1071 (1992).

[23] S. Puri, K. Binder, and S. Dattagupta, Phys. Rev. B **46**, 98 (1992); S. Puri, N. Parekh, and S. Dattagupta, J. Stat. Phys. **75**, 839 (1994).

[24] B. Schmittman and R. Zia, in *Phase Transitions and Critical Phenomena*, edited by C. Domb and J. L. Lebowitz (Academic, London, 1995), Vol. 17.

[25] F. Alexander, C. A. Laberge, J. L. Lebowitz, and R. K. P. Zia, J. Stat. Phys. **82**, 1133 (1996).

[26] E. Levine, Y. Kafri, and D. Mukamel, Phys. Rev. E **64**, 026105 (2001).

[27] A. Achahbar, P. L. Garrido, J. Marro, and M. A. Muñoz, Phys. Rev. Lett. **87**, 195702 (2001).

[28] E. V. Albano and G. Saracco, Phys. Rev. Lett. **88**, 145701 (2002).

[29] P. I. Hurtado, J. Marro, and E. V. Albano, Europhys. Lett. **59**, 14 (2002).

[30] Some partial, unconclusive studies about interfaces in the driven lattice gas (Ref. 31) have been reviewed in Ref. 21.

[31] K.-t. Leung, K. K. Mon, J. L. Valles, and R. K. P. Zia, Phys. Rev. Lett. **61**, 1744 (1988); Phys. Rev. B **39**, 9312 (1989).

[32] This corresponds to the standard Monte Carlo method only if the time increment Δt is drawn from a Poisson distribution. Taking constant $\Delta t = \eta(t)^{-1}$ involves some approximation. However, if the number of particle-hole pairs in the system is sufficiently large, the approximation is excellent. In particular, for a half filled system subject to an *infinite* drive (our model case), the minimum amount of particle-hole pairs present in the system will be of order $2L_{\parallel}$, which is large for large lattices.

[33] P. L. Garrido, J. Marro, and R. Dickman, Ann. Phys. (N.Y.) **199**, 366 (1990).

[34] See, for instance, N. T. J. Bailey, *The Elements of Stochastic Processes* (Wiley, New York, 1964).

[35] A. Guinier and G. Fournet, *Small Angle Scattering of X-Rays* (Wiley, New York, 1955).

[36] O. Penrose, J. L. Lebowitz, J. Marro, M. H. Kalos, and A. Sur, J. Stat. Phys. **19**, 243 (1978); see also O. Penrose, J. L. Lebowitz, J. Marro, M. H. Kalos, and J. Tobochnik, *ibid.* **34**, 399 (1984).

[37] F. de los Santos, P. L. Garrido, and M. A. Muñoz, Physica A **296**, 364 (2001); see also P. L. Garrido, M. A. Muñoz, and F. de los Santos, Phys. Rev. E **61**, R4683 (2000).

[38] H. K. Janssen and B. Schmittmann, Z. Phys. B: Condens. Matter **64**, 503 (1986); K. Leung and J. L. Cardy, J. Stat. Phys. **44**, 567 (1986); **45**, 1087 (1986).

[39] M. San Miguel and R. Toral, in *Instabilities and Nonequilibrium Structures VI*, edited by E. Tirapegui, J. Martínez, and R. Tiemann (Kluwer Academic, New York, 2001).

[40] A. Chakrabarti, R. Toral, and J. D. Gunton, Phys. Rev. B **39**, 4386 (1989).

[41] T. Kawakatsu and T. Munakata, Prog. Theor. Phys. **74**, 11 (1985).

[42] The $t^{1/3}$ behavior here is in contrast with the logarithmic growth that is assumed to govern a class of lattice models in which coarsening is not a direct consequence of surface tension. See I.

Dornic, H. Chaté, J. Chave, and H. Hinrichsen, Phys. Rev. Lett. **87**, 045701 (2001).

[43] More properly, one should speak here of ''self-affinity,'' given the underlying anisotropy (Ref. 19).

[44] Extending some of our arguments to $\rho \neq \frac{1}{2}$ needs some care but the whole picture should still be valid, at least not far from $\rho = \frac{1}{2}$.

[45] Note that the Lifshitz-Slyozov-Wagner behavior is known to be valid in some cases in both $d=2$ and $d=3$ (Ref. 5).

[46] T. Mullin, Phys. Rev. Lett. **84**, 4741 (2000); P. M. Reis and T. Mullin, *ibid.* **89**, 244301 (2002).